Assessment of the Basis-Set Effect on the Structural and Electronic Properties of Organic-Protected Gold Nanoclusters

Francesco Muniz-Miranda,* Maria Cristina Menziani, and Alfonso Pedone

University of Modena and Reggio Emilia (UniMoRE), Department of Chemical and Geological Sciences (DSCG), Via G. Campi 103, I-41125, Modena, Italy

E-mail: francesco.munizmiranda@unimore.it

*To whom correspondence should be addressed

Abstract

Here we have investigated the structural and optical properties of five monolayer-protected gold nanoclusters with a combination of exchange-correlation functionals, namely B-PBE for the geometry relaxation and CAM-B3LYP for the time-dependent calculations.

We have tested the accuracy of five different basis sets in reproducing the experimental structures of these nanoclusters, and we have found that even a rather small basis set (single zeta) can outperform a significantly larger one (double zeta) if some selected atoms are treated with polarization functions. Namely, the sulfur and phosphorous atoms of the capping thiols and phosphines usually are hypervalent when bonded to the gold inner core, therefore polarization functions allow them significantly more structural flexibility. With the two best performing basis sets we carried out optical calculations and found that the resulting UV-Vis profiles are largely similar, in particular for low energy transitions. In particular, the energy and orbital contributions of the optical gaps are very close.

The results support the use of the small basis set proposed here to investigate larger nanoclusters with hybrid and range-corrected functionals.

Introduction

Monolayer-protected Nanoclusters (NCs) with a noble-metal core are particles with single-digit nanometer diameters cupped by organic ligands. They are of great interest for a great number of scientific and technological applications due to their peculiar properties in catalysis,[1,2] their possible interaction with biological substrates,[3] and their optical features.[4] These nanoclusters do not show metallic properties, exhibiting discrete optical gaps (usually between 1 and 2 eV) instead.[5–7] The production of several atomically precise and reproducible nanoclusters with definite structures, which have been determined by X-ray diffraction techniques, has recently been achieved thanks to improvements in the synthesis and crystallization techniques.[8–11]

In turn, the availability of accurate structures allows performing computational studies to elucidate the correlation between size, stoichiometry and optical features of these nano-objects.[7,12–18]

Furthermore, the effect of the organic coatings can be selectively investigated too.[19–21]

Most synthesized monolayer-protected gold NCs are stabilized by thiolate ligands forming complex gold-thiolate interfaces as a consequence of the strong Au-S bond.[22–24] A number of gold clusters stabilized by phosphine ligands have been also synthesized and characterized, including the well-studied undecagold Au_{11} clusters, the icosahedral Au_{13} cluster coordinated by phosphine and halide ligands[25,26] and the $[Au_{39}(PPh_3)_{14}Cl_6]Cl_2$ cluster.[27]

Gold-based NCs are often rationalized within the so called "superatom" theoretical framework:[7] with this approach, the gold core is viewed as a giant atom surrounded by almost-free electrons if the number n^* is equal to the "magic numbers" 8, 16, 20, ... The integer number n^* is given by

$$n^* = (N\nu)_{\mathrm{Au}} - W - q \quad , \tag{1}$$

with N and ν the total number and the atomic valence of Au atoms, respectively, W the total number of monovalent electron-withdrawing groups bound to gold atoms, and q the overall charge of the complex in units of unsigned electrons ($|e|$). This approach has been recently extended to silver-based NCs too,[28] but it still retains several limitations because it has a low predictive power and is limited to particles with spherical or almost-spherical noble metal cores. For example, it cannot be applied to NCs that are prolate[9] or are composed by more than one interacting metal core.

Therefore, at present only an approach based on density functional theory[29] (DFT) and its time-dependent extensions[30] (TD-DFT) can provide quantitative information, in principle regardless of size and shape of the particle. While the latter point is true in theory, this approach is actually limited by the number of atoms in the systems, due to the high computational requirements needed to carry out DFT calculations. Hence, some significant approximations have to be introduced in order to study large NCs at the DFT level of theory .

In the past, DFT and TD-DFT investigations have been carried out on particles ranging between 11 to 102 gold atoms[7,12–14,24,31–37] . However, most of those studies employed plane waves as basis sets: while plane waves form an orthonormal basis, thus immune to basis set superposition errors,

in their actual implementations they only allow adopting simple functionals within the generalized gradient approximation (GGA). Only recently more advanced hybrid and range-corrected hybrid functionals have been adopted to study gold-based NCs[20,21,38] in combination with Gaussian basis sets.

In this study, we investigate the use of a small Gaussian basis set for gold atoms and ligands in five nanoclusters. Adopting it, calculations of structural properties of Au-based NCs larger than Au_{25} and their optical response with the range-corrected hybrid CAM-B3LYP functional can become feasible.

Investigated Nanoclusters

In this paper we have studied five Au-based NCs ranging from Au_{11} to Au_{38}. In particular, two Au_{11}-based NCs with the same metal core[11,19] but different types of ligands have been investigated, one Au_{24}^{+} and a Au_{25}^{2+} NCs[9,39] sharing the position of 24 gold atoms (only the central Au atoms differs), being present in the Au_{25}^{2+} structure and lacking in Au_{24}^{+}), and one Au_{38} NC,[40] thus spanning both neutral and charged particles. The structure of the NCs simulated here are reported in Figure 1. Some of these NCs have been previously studied with DFT methods,[13,20,21,36,38] and here we want to compare the results obtained with a suitable small Gaussian basis set with those obtained with larger Gaussian bases. The two Au_{11}-based NCs can be viewed as superatoms with 8 (almost) free electrons, thus resembling the outer orbital shell of noble gas elements, whereas the other three cannot be rationalized as such, since they are far from being spherical.

In order to speed up our computations, in calculations on the Au_{11}, Au_{24}^{+} and Au_{25}^{2+} NCs only the metal core and the atoms directly bonded to them (saturated by H atoms in order to complete their valence) were retained. Thus, the aromatic thiols (SPh) and phosphines (PPh_3) that protect these gold cores are largely omitted. This simplification scheme has been widely applied before[7,12,24,31,32] and validated at least for the cluster composed by 11-25 gold atoms.[20,21,38] For the Au_{38} NC, since the gold core is capped with SC_2H_4Ph thiols, the ligands are substituted with

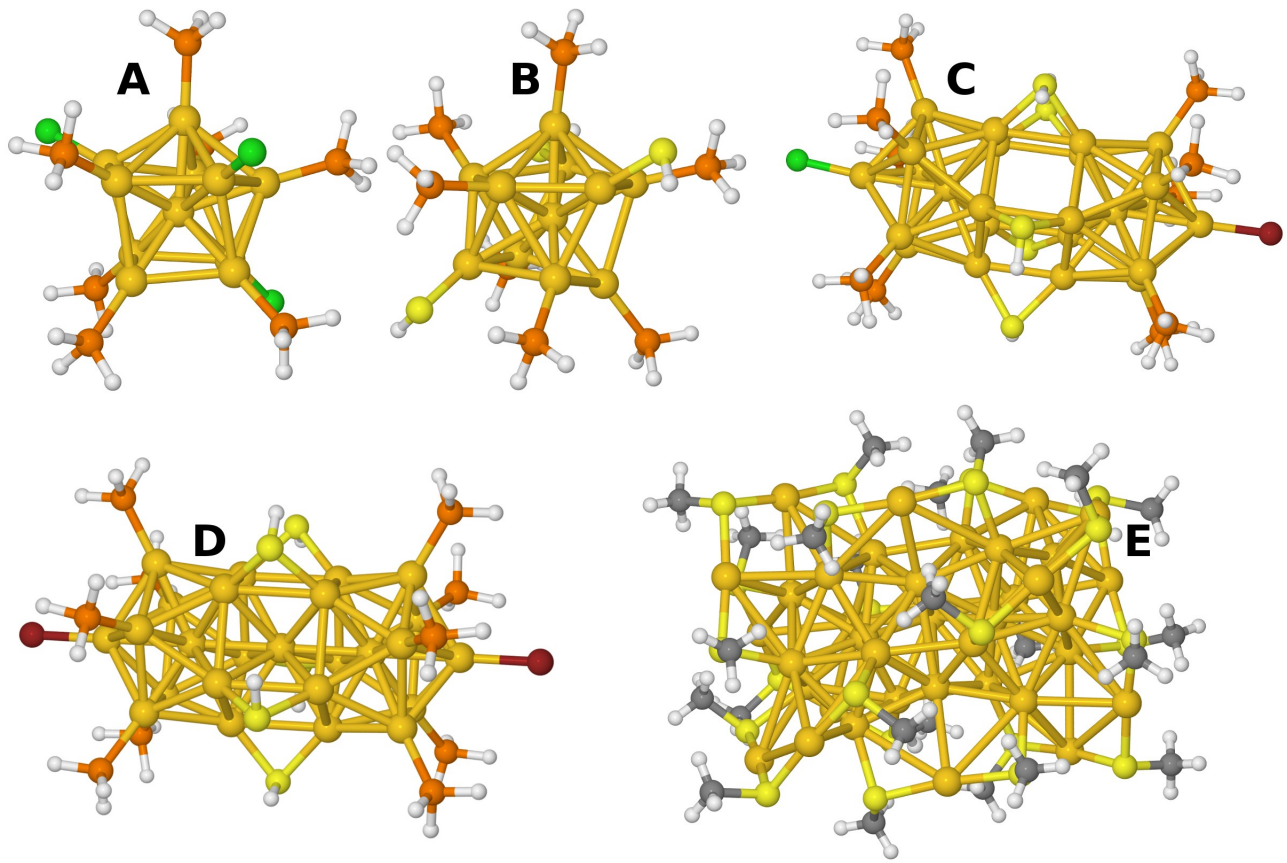

Figure 1: Nanoclusters investigated here. (**A**) $Au_{11}(PH_3)_7Cl_3$, hereafter referred to as $Au_{11}(1)$. (**B**) $Au_{11}(PH_3)_7(SH)_3$, hereafter referred to as $Au_{11}(2)$. (**C**) $Au_{24}(PH_3)_{10}(SH)_5ClBr^+$. (**D**) $Au_{25}(PH_3)_{10}(SH)_5Br_2^{2+}$. (**E**) $Au_{38}(SCH_3)_{24}$.

S-CH_3 groups.

Methods and Computational Details

All calculations were performed with the Gaussian 09 (release D) suite of programs,[41] in combination with the generalized gradient approximated B-PBE[42,43] exchange-correlation (XC) functional for structural optimization and the range separated hybrid XC functional CAM-B3LYP[44] for TD-DFT optical excitations, carried out within the linear response scheme. These functionals have been previous validated on gold NCs as able to correctly reproduce the structure and the UV-Vis spectra, respectively.[20,21] Self-consistent-field and optimization convergence criteria have been set at the "tight" level of accuracy. Optical transitions were convoluted into spectra with the Gaussview

software.[45] Orbital isosurfaces were also plotted with the software Gaussview and structures with Jmol[46] adopting the standard CPK color code. The electronic density of states analysis was performed with the Multiwfn software.[47,48]

We have tested a mixed combined Gaussian basis set and electronic core potential (ECP) to perform fast simulation on a range of Au-based nano-objects of different complexity, shape and charge state. Namely, we have used the small LanL2-MB[49,50] basis set to simulate gold atoms: this basis set adopts the LanL2 ECP for core electrons in combination with a STO-3G minimal basis set for valence electrons; atoms bonded to the metal core have been described with the 6-21G* basis set and all other atoms with the STO-3G basis set. For reason of shortness, hereafter we refer to this mixed LanL2-MB/6-21G*/STO-3G basis set as LanL2-MB*.

This choice of basis set has been compared with calculations (geometrical optimizations with B-PBE functional) performed with different bases on the two Au_{11}, Au_{24}^{+}, and Au_{25}^{2+} NCs:

- full LanL2-MB on all atoms.
- full LanL2-DZ[49,51,52] on all atoms.
- modified LanL2-DZ[53] on gold atoms (which adds diffuse $|p>$ orbitals to LanL2-DZ), 6-21G* on atoms bonded to the gold cores and STO-3G on all other atoms. This basis set shall be hereafter referred to as mod-LanL2-DZ* and has been included thanks to the `Basis Set Exchange` database.[54]

The use of the modified LanL2-DZ to describe Au atoms has been suggested in Ref. 20 as one of the best ones to correctly reproduce the structural features of Au-based NCs.

We have then employed mod-LanL2-DZ* and LanL2-MB* bases to study the optical properties of the NCs at the TD-CAM-B3LYP level of theory. As an application, the LanL2-MB* basis set has then been applied to the Au_{38}-based NC to analyze its structural and optical features.

Results and Discussions

Structural Features

The clusters have been structurally optimized with the B-PBE functional, as described in the previous section. Five different basis sets have been employed for checking their accuracy in maintaining the experimental geometry. In order to evaluate this accuracy, the atom-averaged unsigned displacement ($< \delta >$) of the relaxed structure (*opt*) with respect to the experimental structure (*exp*) has been computed as

$$< \delta > = < |r_{ij}^{exp} - r_{ij}^{opt}| > \quad ,$$

where r_{ij} represents the distance between i and j metal atoms, as previously done in Ref. 20. The results of these optimizations are summarized in Table 1, while in Table 2 the time required to achieve wavefunction convergence with the various basis sets are reported for the smallest cluster.

Table 1: Mean unsigned error of the optimized structures of the five NCs with 4 different combination of basis sets. Values are reported in Å.

$< \delta >$/Å	**LanL2-MB**	**LanL2-DZ**	**mod-LanL2-DZ***	**LanL2-MB***
Au_{11} (1)	> 0.25	0.17	0.02	0.04
Au_{11} (2)	> 0.25	0.16	0.02	0.03
Au_{24}^{+}	> 0.25	0.22	0.06	0.07
Au_{25}^{2+}	> 0.25	0.19	0.05	0.07
Au_{38}	—	—	—	0.12

Table 2: Time to achieve self consistent field convergence (standard Gaussian 09 "tight" criteria) on a machine made up of two 8-Core Intel Xeon E5-2670 clocked at 2.60 GHz with 24 GB of random access memory and an hard disk at 7200 RPM. The time is reported in minutes.

time / min	**LanL2-MB**	**LanL2-DZ**	**mod-LanL2-DZ***	**LanL2-MB***
Au_{11} (1)	8.3	17.6	27.9	9.4

As can be appreciated, the LanL2-MB basis set yields the worse structures, which is not unexpected since it is also the smallest basis set investigated here. We have to pinpoint that values

of $< \delta >$ parameter larger than 0.15Å are associated to appreciably distorted final geometries, and values larger than 0.25Å usually mean that the network of Au-Au bonds is at least partially destroyed: as a guide for the eye, this can be observed in Figure 2 comparing an optimization with $< \delta >> 0.25$ (left) and one with $< \delta > \sim 0.02$ (right).

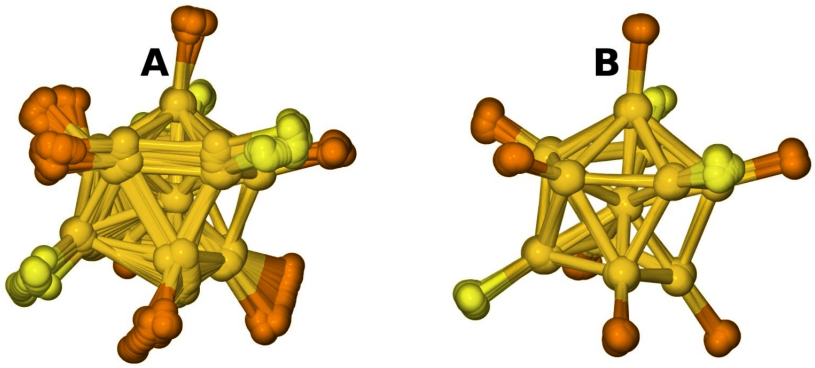

Figure 2: Superimposed experimental and relaxed structures of $Au_{11}(2)$. (**A**) Computed with the LanL2-MB basis set. (**B**) Computed with the mod-LanL2-DZ* basis set.

LanL2-DZ gives results of greater accuracy, and even more so the mod-LanL2-DZ*, which was already proved to be one of the most accurate Gaussian basis set for gold NCs in previous works.[20,21,38,55] However, LanL2-MB* yields optimized structures of fair accuracy, better than the larger LanL2-DZ. For the smallest NC studied here, namely $Au_{11}(1)$, we observe that LanL2-MB* and LanL2-MB require about half the time of LanL2-DZ to achieve wavefunction convergence, which corresponds to about one third of the time required with mod-LanL2-DZ*. Thus, overall, LanL2-MB* seems a reasonable trade off between accuracy and the computation resources required to run the calculations.

This could be somewhat surprising since basically LanL2-MB and LanL2-MB* differ only in the treatment of the atoms directly bonded to the gold cores (S, P, Cl, and Br atoms in the five NCs investigated here). With the pure LanL2-MB a STO-3G basis set is employed on them (from third and fourth row elements also the LanL2 ECP is also adopted), whereas with LanL2-MB* a polarized 6-21G* basis is used on them. To assess if the the improved accuracy in the passage STO-3G $\rightarrow$ 6-21G* is due to the change from single to double zeta basis or to the adding of polarization functions, we also performed geometry relaxation on the two Au_{11} clusters with a

basis set identical to LanL2-MB* but with 6-21G functions on atoms bonded to the Au cores, thus dropping the polarization functions. With this choice, we observed values of $< \delta >$ parameter of 0.22 and 0.23 for $Au_{11}(1)$ and $Au_{11}(2)$ NCs, respectively, worse than what is obtained with LanL2-DZ basis set and only slightly better than what obtained with LanL2-MB.

Hence, structural optimizations can be improved not only adding diffuse functions on the gold cores, as done with the modified LanL2-DZ combined ECP and basis set (as observed in Ref.s 20,21,38,55), but also adding polarization functions on the nearby atoms. This is most likely due to the fact that Au cores are often bonded to thiols and phosphines, and both S and P atoms are usually hypervalent in these cases and thus polarization functions allow them to relax towards more realistic geometrical conformations.

Optical and Electronic Properties

The electronic and optical features of the five NCs has been computed at the CAM-B3LYP and TD-CAM-B3LYP level of theory with the LanL2-MB* basis set and compared with those obtained with mod-LanL2-DZ*.

First, we have investigated the charge redistribution in the NCs with the two basis sets in terms of Hirshfeld partial charges,[56] since they are less sensitive to the basis set employed and were already reported in literature.[20,38] It can be observed that both of them predict the same sign of the charge for homologous atoms even if the two basis sets yield different partial charges. As a comparison, it has to be kept in mind that similar calculations adopting the same basis set but different functionals may yield for the same atom a severely positive or negative net charge (see for example Ref. 20). Furthermore, both basis sets predict the same qualitative trend in the distribution of charge: in particular, it has been found[20,38] that inner gold atoms (i.e. Au atoms bonded only to other Au atoms) are significantly less negatively charged than metal atoms on the surface, a behavior reproduced by both LanL2-MB* and mod-LanL2-DZ*. In any case, the average gold charges computed with LanL2-MB* are about 60-70% of those computed with mod-LanL2-DZ*.

We also analyzed the energy of the first optical transition ($S_1 \leftarrow S_0$), which corresponds to the

Table 3: Hirshfeld partial charges in units of $|e|$, with e being the electron charge.Calculations were performed at the CAM-B3LYP level of theory. All data are averaged on the specified type of atoms, unless a the label "inner atom" is reported: a Au "inner atom" is a gold atom surrounded only by other Au atoms.

	mod-LanL2-DZ*	LanL2-MB*
Au_{11} (1)		
Au	-0.116	-0.085
Au (inner atom)	-0.043	-0.008
P	0.352	0.320
Cl	-0.401	-0.473
Au_{11} (2)		
Au	-0.189	-0.109
Au (inner atom)	-0.059	-0.011
P	0.294	0.209
S	-0.236	-0.259
Au_{24}^{+}		
Au	-0.076	-0.062
Au (inner atoms)	-0.024	-0.010
Br/Cl	-0.431	-0.476
P	0.362	0.354
S	0.015	-0.034
Au_{25}^{2+}		
Au	-0.080	-0.045
Au (inner atoms)	-0.004	-0.008
Br	-0.314	-0.421
P	0.359	0.383
S	0.033	0.013
Au_{38}		
Au	—	-0.045
Au (inner atoms)	—	-0.004
S	—	0.017

so called "optical gap" of the cluster,[20,57,58] as reported in Table 4. As can be noticed, calculations with mod-LanL2-DZ* and LanL2-MB* basis sets yields very similar optical gaps, with a maximum difference of $\sim$0.15 eV for the Au_{25}^{2+}-based NC; for the Au_{11} and Au_{24}^{+}-based NCs the difference is only $<$0.10 eV. Moreover, calculations performed with the LanL2-MB* basis, despite its limitations, yield values slightly closer to the experimental data (when the latter ones are available, namely for Au_{11}(1), Au_{24}^{+}, and Au_{25}^{2+} NCs). It has to be noticed that for Au_{24}^{+} it is difficult to extrapolate the true optical gap, because of some contradicting data between optical and elec-

Table 4: Optical gaps of the nanoclusters.

Energy / eV	**mod-LanL2-DZ***	**LanL2-MB***	**Exp**	
Au_{11} (1)	2.86	2.77	∼2.1	Ref. 19
Au_{11} (2)	2.62	2.64	—	
Au_{24}^{+}	2.05	2.04	1.3 - 1.9	Ref.s 9,20
Au_{25}^{2+}	2.21	2.07	1.79	Ref. 39
Au_{38}	—	1.33	—	

trochemical measurements.[9,20] We have also to pinpoint that with the LanL2-MB* basis set the energy of the optical gap appears shrinking with the increase of the particle size, something that could qualitatively be expected since larger particles should have optoelectronic properties closer to those of bulk gold rather than sub-nanometer NCs.

The $S_1 \leftarrow S_0$ excitations can also be investigated on the basis of the most relevant orbital contributions to them, and computations with both mod-LanL2-DZ* and LanL2-MB* show that the LUMO←HOMO transition is the main component; Figure 3 reports the frontier orbitals for $Au_{11}(1)$ with the two basis sets. In the case of Au_{24}^{+} and Au_{25}^{2+} also the LUMO←HOMO-1 transitions give an appreciable contribution (about 40% of the LUMO←HOMO contribution), while for the Au_{38}-based NC the LUMO+1←HOMO-1 one gives a very important contribution (about 80% of the LUMO←HOMO).

Another important feature of these gold NCs is the energy of the first charge-transfer excitation, namely the first ligand←core band. For NCs $Au_{11}(1)$ and $Au_{11}(2)$ it was already established[21] that the first of such excitations occur at ∼4.83 eV (LUMO+10←HOMO) and ∼4.27 eV (LUMO+6←HOMO-2), respectively, at the TD-CAM-B3LYP level of theory with a basis set very similar to mod-LanL2-DZ*. Even if the ligands here are mostly omitted, this comparison can still be carried out at least in a qualitatively fashion, as we report here for $Au_{11}(1)$. The first charge-transfer excitation with mod-LanL2-DZ* occurs at ∼5.06 eV, and is mainly of the type LUMO+10←HOMO-1, while with LanL2-MB* it occurs at ∼4.95 eV and is mainly of the type LUMO+11←HOMO. The orbitals involved in this transition are reported in Figure 4. While the orbitals are somewhat different, and the transition energies differs of ∼0.11 eV, they are still qual-

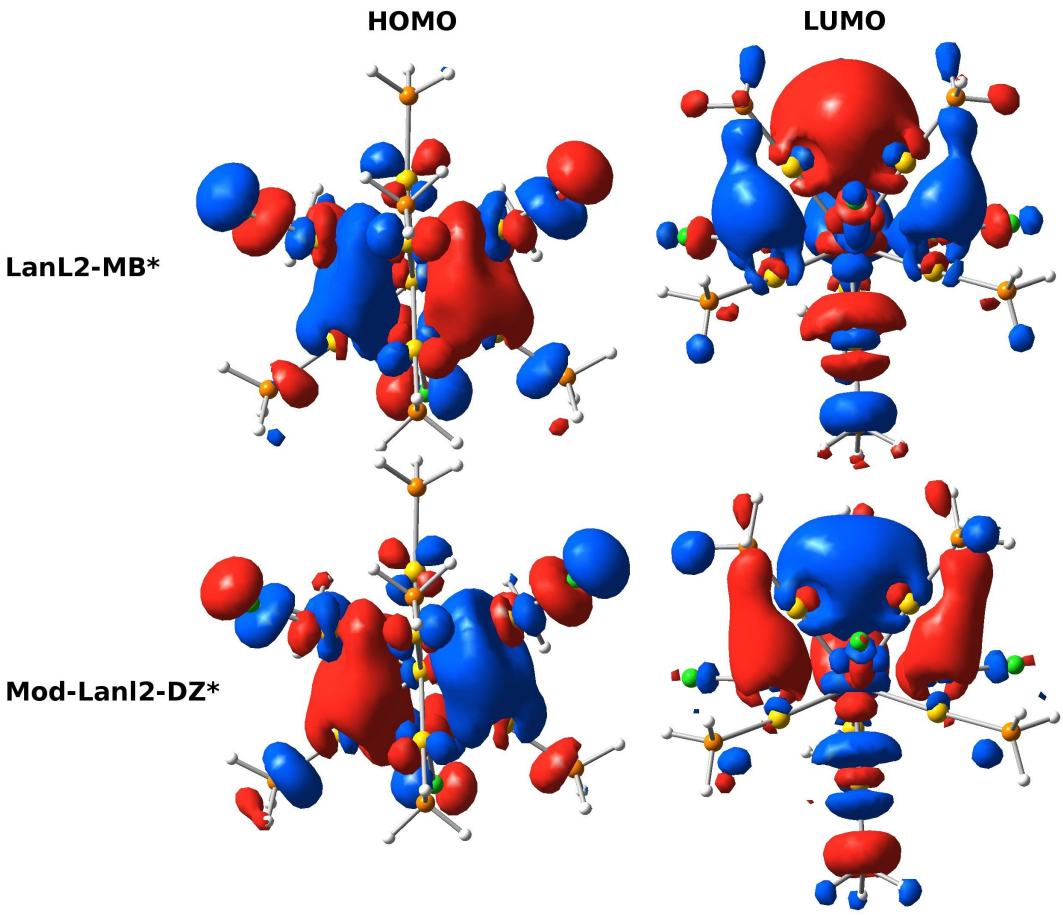

Figure 3: Isosurfaces of the frontier orbitals of $Au_{11}(1)$, computed with both the mod-LanL2-DZ* and LanL2-MB* basis sets.

itatively close.

This latter point could also be assessed by comparing the optical spectra calculated with the two basis sets, as reported in Figure 5. A redshift with the size increase is particularly evident, as discussed before about the optical gaps. For all the NCs for which a comparison is possible, the overall shapes of the spectra computed with the two basis sets seems very similar, in particular for the fist low energy bands. For $Au_{11}(1)$ this is very noticeable. The shape yielded with LanL2-MB* seems slightly more structured (in particular for $Au_{11}(2)$ and Au_{25}^{2+}), suggesting that the LanL2-MB* excitations are less uniformly distributed at high energy. In fact, the spike transitions are less similar, suggesting that the nest of excitations are somewhat different even if they yield very similar smoothed spectra. However, some transitions are clearly recognizable as just being red or

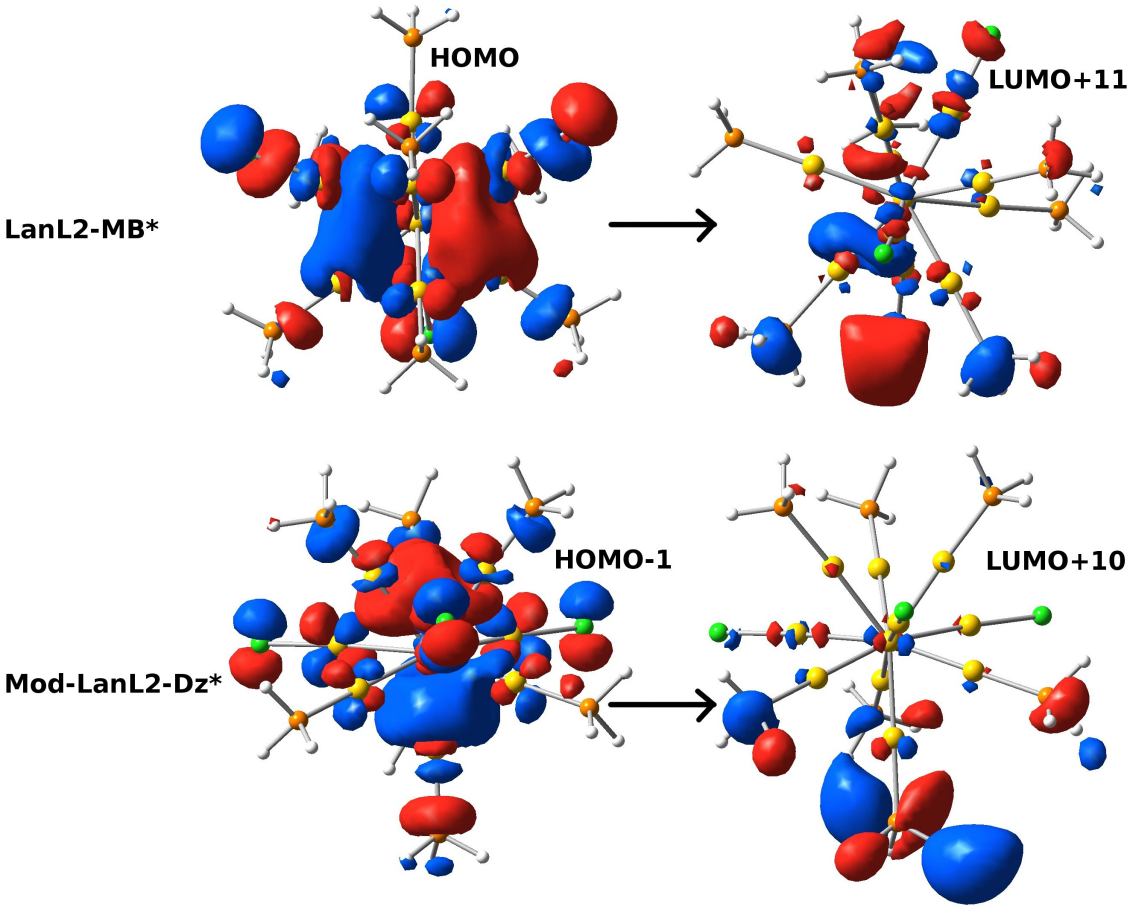

Figure 4: Isosurfaces of the orbitals involved in the first charge transfer transition (ligand←core) with the mod-LanL2-DZ* and LanL2-MB* basis sets of the $Au_{11}(1)$ NC.

blue shifted with respect to one basis set. Unfortunately, it seems not possible to predict if LanL2-MB* excitations are red or blue-shifted with respect to those computed with the mod-LanL2-DZ*: for example, they are blue-shifted for $Au_{11}(2)$ but they are red-shifted for Au_{25}^{2+}; this impairs the possibility to systematically translate the excitations computed with LanL2-MB* of a known factor to match the others.

The spectrum of Au_{38} appears largely similar to that of the Au_{25}^{2+} NC, which is reasonable since both of them are basically made up of two subunits (two Au_{11} for Au_{25}^{2+}, and two Au_{13} for Au_{38}). Figure 5. The electronic density of states (eDoS), pictured in Figure 6, displays a very small band-gap, which is qualitatively consistent with the shrinking of the optical gap with the increase in particle size. Eigenstates localized on S atoms (in yellow in Figure 6) give little contributions

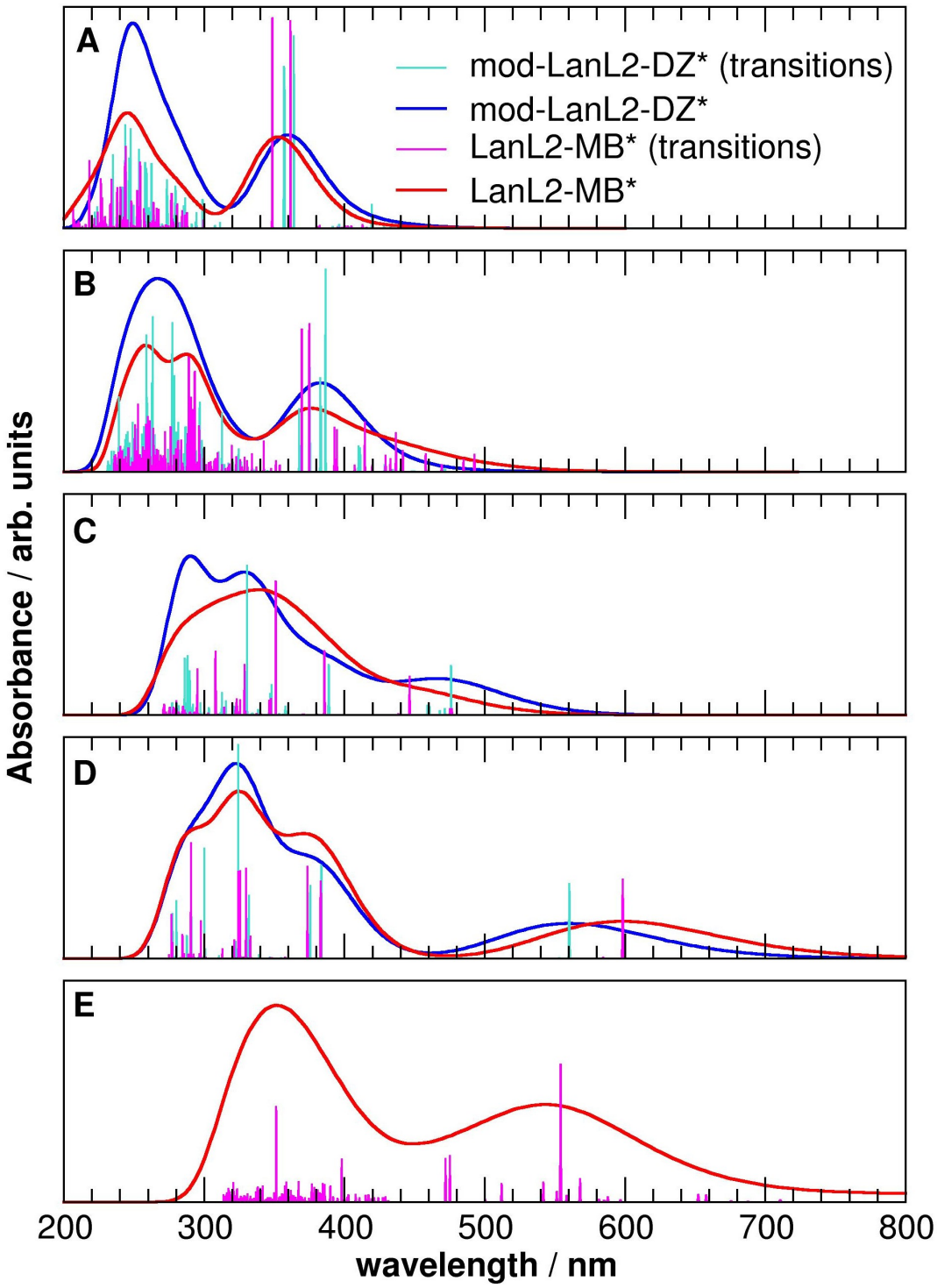

Figure 5: Computed TD-CAM-B3LYP spectra (200 excitations) of the $Au_{11}(1)$ (**A**), $Au_{11}(2)$ (**B**), Au_{24}^{+} (**C**), Au_{25}^{2+} (**D**), and Au_{38} (**E**) NCs. In blue and red are reported the spectra smoothed with Gaussian functions with half-width at half-maximum of 0.25 eV, while in cyan and magenta the actual transitions.

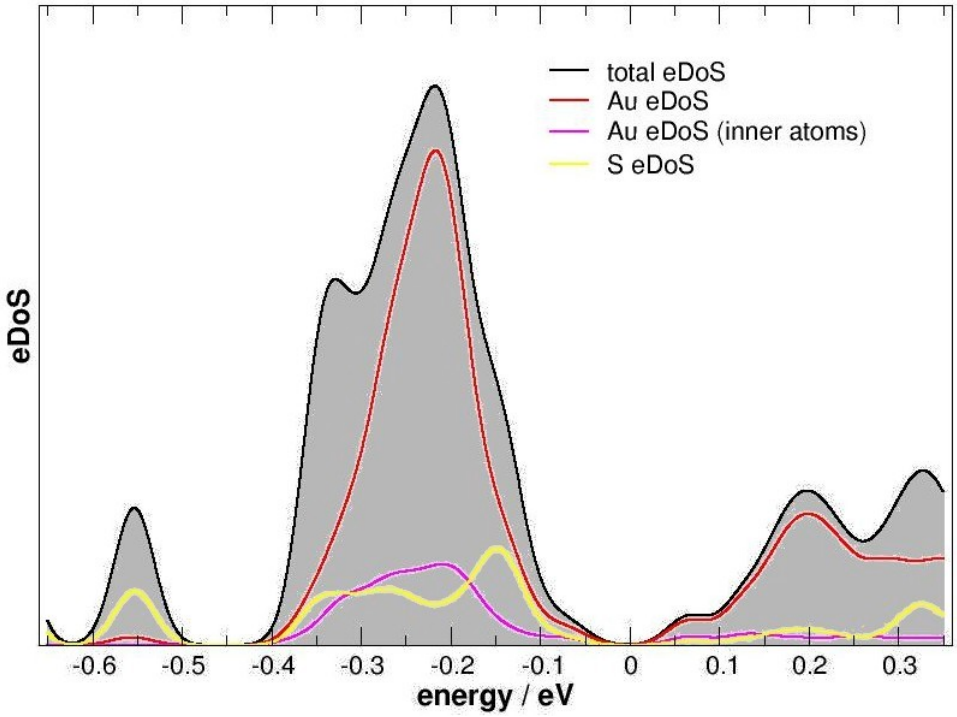

Figure 6: Electronic density of states of the Au_{38}-based NC. The eDoS has been translated to have the band-gap at 0 eV. The eDoS has been smoothed with Gaussian functions with half-width at half-maximum of 0.05 Hartree.

to virtual orbitals close to the band-gap, while they are important to the occupied orbitals. Orbitals on the inner gold atoms (in magenta in Figure 6) give almost no contribution to virtual orbitals and are significant just for occupied orbitals distant 0.2 eV from the band-gap. Thus, the first optical excitations mainly involve surface gold atoms and not Au atoms deep into the core of the particle.

Concluding Remarks

In this work we have carried out structural optimizations and optical spectra calculations on five monolayer protected gold-based nanoclusters.

We have employed four different basis sets during the structural optimizations with the B-PBE exchange-correlation functional, to asses which one yielded relaxed structures closer to those resolved by means of X-Ray diffraction. While it has been recovered that solutions based on the modified LanL2-DZ basis give the best accord with the experimental data, we have noted that the much smaller LanL2-MB basis set (readily available in Gaussian 09) can yield structures of similar

accuracy if coupled with a polarized basis set on the atoms bonded to the gold cores (in the case of our tested nanoclusters, namely S, P, Cl). In fact, basis sets larger than LanL2-MB such as the standard LanL2-DZ fail to achieve a similar accuracy because they do not provide polarization functions on those atoms, which are often hypervalent when they are bound to Au atoms. This suggest that a good way to increase the accuracy of structural calculations on monolayer-protected gold nanoclusters is also to improve the description of the "surface" atoms. We thus propose to use the LanL2-MB basis set on Au atoms and a basis like 6-21G* at least on S and P atoms of the cupping ligands.

We have also carried out optical calculations at the TD-CAM-B3LYP level of theory with the basis set based on LanL2-MB and modified LanL2-DZ. Optical gaps are largely similar, both as excitation energy and orbital components. The resulting UV-Vis profiles are largely similar, in particular for the low energy transitions close to the optical gap. In this regard, orbitals close in energy to the HOMO-LUMO gap computed with one basis are basically indistinguishable from those computed with the other one. Also, charge transfer excitations of the type Ligand←Metal are recovered at very similar energies. The higher excitations, however, present some noticeable difference even if when smoothed they still yield more or less the same optical profiles.

Therefore, we suggest the use of small basis set LanL2-MB in combination with a polarized basis set on boundary atoms in order to relax experimental structures and compute optical gaps of gold-based nanoclusters, in lieu of the much larger modified LanL2-DZ basis set. This choice can also be adopted to predict the general shape of the visible absorption bands.

This basis set makes feasible investigating with hybrid and range-separated hybrid exchange-correlation functionals (like the CAM-B3LYP employed here) even larger nanoclusters, whose properties currently have been studied only with simpler generalized gradient approximated functionals and plane wave basis sets.

Acknowledgement

This work was supported by the Italian "*Ministero dell'Istruzione, dell'Università e della Ricerca*" (MIUR) through the ''*Futuro in Ricerca*" (FIRB) Grant RBFR1248UI_002 entitled "Novel Multiscale Theorethical / Computational Strategies for the Design of Photo and Thermo responsive Hybrid Organic-Inorganic Components for Nanoelectronic Circuits", and the "*Programma di ricerca di rilevante interesse nazionale*" (PRIN) Grant 2010C4R8M8 entitled "Nanoscale functional Organization of (bio)Molecules and Hybrids for targeted Application in Sensing, Medicine and Biotechnology" is also acknowledged. CINECA granted computation time within the research project AUNANMR - HP10CJ027S.

References

(1) Campbell, C. T. *Science* **2004**, *306*, 234–235.

(2) Cong, H.; Becker, C. F.; Elliott, S. J.; Grinstaff, M. W.; Porco, J. A. *J. Am. Chem. Soc.* **2010**, *132*, 7514–7518.

(3) Falletta, E.; Bonini, M.; Fratini, E.; Lo Nostro, A.; Pesavento, G.; Becheri, A.; Lo Nostro, P.; Canton, P.; Baglioni, P. *J. Phys. Chem. C* **2008**, *112*, 11758–11766.

(4) Bauld, R.; Hesari, M.; Workentin, M. S.; Fanchini, G. *Nanoscale* **2014**, *6*, 7570–7575.

(5) Chen, S.; Ingram, R. S.; Hostetler, M. J.; Pietron, J. J.; Murray, R. W.; Schaaff, T. G.; Khoury, J. T.; Alvarez, M. M.; Whetten, R. L. *Science* **1998**, *280*, 2098–2101.

(6) Alivisatos, A. P. *J. Phys. Chem.* **1996**, *100*, 13226–13239.

(7) Walter, M.; Akola, J.; Lopez-Acevedo, O.; Jadzinsky, P. D.; Calero, G.; Ackerson, C. J.; Whetten, R. L.; Grönbeck, H.; Häkkinen, H. *Proc. Natl. Acad. Sci. U.S.A.* **2008**, *105*, 9157–9162.

(8) Shichibu, Y.; Negishi, Y.; Tsukuda, T.; Teranishi, T. *J. Am. Chem. Soc.* **2005**, *127*, 13464–13465.

(9) Das, A.; Li, T.; Nobusada, K.; Zeng, Q.; Rosi, N. L.; Jin, R. *J. Am. Chem. Soc.* **2012**, *134*, 20286–20289.

(10) Park, S.; Lee, D. *Langmuir* **2012**, *28*, 7049–7054.

(11) Nunokawa, K.; Onaka, S.; Ito, M.; Horibe, M.; Yonezawa, T.; Nishihara, H.; Ozeki, T.; Chiba, H.; Watase, S.; Nakamoto, M. *J. Organomet. Chem.* **2006**, *691*, 638 – 642.

(12) Häkkinen, H.; Barnett, R. N.; Landman, U. *Phys. Rev. Lett.* **1999**, *82*, 3264–3267.

(13) Goh, J.-Q.; Malola, S.; Häkkinen, H.; Akola, J. *J. Phys. Chem. C* **2013**, *117*, 22079–22086.

(14) Hartmann, M. J.; Häkkinen, H.; Millstone, J. E.; Lambrecht, D. S. *J. Phys. Chem. C* DOI: 10.1021/jp5125475.

(15) Muniz-Miranda, F.; Menziani, M. C.; Pedone, A. *The Journal of Physical Chemistry A* **2015**, *119*, 5088–5098, PMID: 25248052.

(16) Bousquet, B.; Cherif, M.; Huang, K.; Rabilloud, F. *J. Phys. Chem. C* **2015**, *119*, pp 4268–4277.

(17) Barcaro, G.; Sementa, L.; Fortunelli, A.; Stener, M. *J. Phys. Chem. C* **2014**, *118*, 12450–12458.

(18) Barcaro, G.; Sementa, L.; Fortunelli, A.; Stener, M. *J. Phys. Chem. C* **2014**, *118*, 28101–28108.

(19) Gutrath, B. S.; Englert, U.; Wang, Y.; Simon, U. *European Journal of Inorganic Chemistry* **2013**, *2013*, 2002–2006.

(20) Muniz-Miranda, F.; Menziani, M. C.; Pedone, A. *J. Phys. Chem. C* **2014**, *118*, 7532–7544.

(21) Muniz-Miranda, F.; Menziani, M. C.; Pedone, A. *Phys. Chem. Chem.Phys.* **2014**, *16*, 18749–18758.

(22) Jadzinsky, P. D.; Calero, G.; Ackerson, C. J.; Bushnell, D. A.; Kornberg, R. D. *Science* **2007**, *318*, 430–433.

(23) Maksymovych, P.; Sorescu, D. C.; Yates, J. T. *Phys. Rev. Lett.* **2006**, *97*, 146103.

(24) Häkkinen, H. *Nature Chemistry* **2012**, *4*, 443–455.

(25) Shichibu, Y.; Kamei, Y.; Konishi, K. *Chem. Commun.* **2012**, *48*, 7559–7561.

(26) Das, A.; Li, T.; Li, G.; Nobusada, K.; Zeng, C.; Rosi, N. L.; Jin, R. *Nanoscale* **2014**, *6*, 6458–6462.

(27) Teo, B. K.; Shi, X.; Zhang, H. *Journal of the American Chemical Society* **1992**, *114*, 2743.

(28) Goh, J.-Q.; Akola, J. *The Journal of Physical Chemistry C* **2015**, *119*, 21165–21172.

(29) Parr, R. G.; Yang, W. *Density-Functional Theory of Atoms and Molecules*; Oxford University Press, 1994.

(30) Runge, E.; Gross, E. K. U. *Phys. Rev. Lett.* **1984**, *52*, 997–1000.

(31) Aikens, C. M. *J. Phys. Chem. C* **2008**, *112*, 19797–19800.

(32) Zhu, M.; Aikens, C. M.; Hollander, F. J.; Schatz, G. C.; Jin, R. *J. Am. Chem. Soc.* **2008**, *130*, 5883–5885.

(33) Provorse, M. R.; Aikens, C. M. *J. Am. Chem. Soc.* **2010**, *132*, 1302–1310.

(34) Hulkko, E.; Lopez-Acevedo, O.; Koivisto, J.; Levi-Kalisman, Y.; Kornberg, R. D.; Pettersson, M.; Häkkinen, H. *Journal of the American Chemical Society* **2011**, *133*, 3752–3755, PMID: 21348523.

(35) Hadley, A.; Aikens, C. M. *J. Phys. Chem. C* **2010**, *114*, 18134–18138.

(36) Lopez-Acevedo, O.; Tsunoyama, H.; Tsukuda, T.; Häkkinen, H.; Aikens, C. M. *J. Am. Chem. Soc.* **2010**, *132*, 8210–8218.

(37) Aikens, C. M. *J. Phys. Chem. Lett.* **2011**, *2*, 99–104.

(38) Muniz-Miranda, F.; Menziani, M. C.; Pedone, A. *The Journal of Physical Chemistry C* **2015**, *119*, 10766–10775.

(39) Wang, S.; Meng, X.; Das, A.; Li, T.; Song, Y.; Cao, T.; Zhu, X.; Zhu, M.; Jin, R. *Angew. Chem. Int. Ed.* **2014**, *53*, 2376–2380.

(40) Qian, H.; Eckenhoff, W. T.; Zhu, Y.; Pintauer, T.; Jin, R. *Journal of the American Chemical Society* **2010**, *132*, 8280–8281, PMID: 20515047.

(41) Frisch, M. J. et al. *Gaussian 09, Revision D.01*, Gaussian, Inc., Wallingford CT, 2013.

(42) Becke, A. D. *Phys. Rev. A* **1988**, *38*, 3098–3100.

(43) Perdew, J. P.; Burke, K.; Ernzerhof, M. *Phys. Rev. Lett.* **1996**, *77*, 3865–3868.

(44) Yanai, T.; Tew, D. P.; Handy, N. C. *Chem. Phys. Lett.* **2004**, *393*, 51 – 57.

(45) Dennington, R.; Keith, T.; Millam, J. *GaussView Version 5*, Semichem Inc. Shawnee Mission KS 2009.

(46) http://www.jmol.org, version: Jmol 12.2.2+dfsg-1.

(47) Lu, T.; Chen, F. *J. Comput. Chem.* **2012**, *33*, 580–592.

(48) Lu, T.; Chen, F. *Acta Chim. Sinica* **2011**, *69*, 2393–2406.

(49) Dunning Jr., T. H.; Hay, P. J. *J. Chem. Phys.* **1985**, *82*, 270.

(50) Hay, P. J.; Wadt, W. R. *J. Chem. Phys.* **1985**, *82*, 299–310.

(51) Dunning Jr., T. H.; Hay, P. J. *J. Chem. Phys.* **1985**, *82*, 284.

(52) Dunning Jr., T. H.; Hay, P. J. *J. Chem. Phys.* **1985**, *82*, 299.

(53) Couty, M.; Hall, M. B. *J. Comput. Chem.* **1996**, *17*, 1359–1370.

(54) Schuchardt, K.; Didier, B.; Elsethagen, T.; Sun, L.; Gurumoorthi, V.; Chase, J.; Li, J.; Windus, T. *J. Chem. Inf. Model.* **2007**, *47*, 1045–1052.

(55) Goel, S.; Velizhanin, K. A.; Piryatinski, A.; Tretiak, S.; Ivanov, S. A. *J. Phys. Chem. Lett.* **2010**, *1*, 927–931.

(56) Hirshfeld, F. *Theor. Chim. Acta* **1977**, *44*, 129–138.

(57) Kronik, L.; Stein, T.; Refaely-Abramson, S.; Baer, R. *J. Chem. Theory Comput.* **2012**, *8*, 1515–1531.

(58) Baerends, E. J.; Gritsenko, O. V.; van Meer, R. *Phys. Chem. Chem. Phys.* **2013**, *15*, 16408–16425.